Characterization of the collisionally pumped optical-field-ionized soft-x-ray laser at 41.8 nm driven in capillary tubes

B. Cros,[1] T. Mocek,[2,*] I. Bettaibi,[2] G. Vieux,[1] M. Farinet,[1] J. Dubau,[3] S. Sebban,[2] and G. Maynard[1]
[1]*Laboratoire de Physique des Gaz et des Plasmas, CNRS-UMR8578, bat. 210, Université Paris XI, 91405 Orsay, France*
[2]*Laboratoire d'Optique Appliquée (LOA), ENSTA-École Polytechnique, Chemin de la Hunière, 91761 Palaiseau, France*
[3]*Laboratoire d'Interaction du Rayonnement X avec la Matière, Bât, 350, Université Paris-Sud, 91405 Orsay, France*
(Received 28 October 2005; published 2 March 2006)

We report on experimental and theoretical studies of a collisionally pumped, optical-field-ionized soft-x-ray laser (SXRL) at 41.8 nm driven in capillary tubes with smooth inner surface. A detailed experimental study has been conducted in order to understand the key effects related to guiding in this configuration. The amplifying plasma was created inside few-cm-long capillary tubes, and maximum extreme ultraviolet emission was obtained when operating in a multimode guiding regime with an optimized lasing signal from a 25-mm-long capillary a factor of 3 higher than that of a gas cell and with a beam divergence reduced by a factor of 3. A numerical code, named COFIXE, has been developed to calculate the SXRL signal emitted by the plasma source. It includes the calculation of the pump beam propagation, the determination of the plasma state just after the interaction with the pump beam, the calculation of the evolution of the local properties of the plasma during the subsequent few ps, and the calculation of the amplification and transport of the SXRL emission. Excellent agreement has been obtained between experiment and theory for several features such as the divergence of the beam, the correlation between guided pump beam transmission and SXRL energy, and the enhancement factor induced by guiding.

DOI: 10.1103/PhysRevA.73.033801 PACS number(s): 42.55.Vc, 52.38.Hb

I. INTRODUCTION

Optical-field-ionized (OFI), collisionally excited soft-x-ray laser (SXRL) systems can be achieved with compact pump lasers at repetition rates of a few Hz. In this scheme, an intense, short, circularly polarized pump laser pulse is used to ionize a gas target and create a nonequilibrium plasma in which population inversion between excited states of specific ionic species can be obtained. The ionization stage and the electron distribution in energy are both controlled by pump laser parameters.

The OFI SXRL was first demonstrated in Pd-like xenon with a transition at 41.8 nm by Lemoff and co-workers in 1995 [1]. Since then, important progress has been achieved: saturated amplification at 41.8 nm has been obtained [2] in Xe^{8+}, and the OFI SXRL technique has been extended to the use of Ni-like krypton with the observation of a strong amplification at 32.8 nm [3].

In these demonstrations a low-density plasma ($\sim 10^{18}$ cm^{-3}) was created in gas cells over a distance of the order of a few Rayleigh lengths. A circularly polarized laser beam with an intensity of $1-5\times 10^{17}$ W cm^{-2} was used to obtain the required degree of ionization of the ionic species by OFI. The circular polarization enables efficient heating of the free electrons to create the population inversion by collisions with the bound electrons of the Xe^{8+} or Kr^{8+} species. One limitation of this scheme is the short length of the amplification medium limited typically to a few mm. To extend the length of the lasing medium it is necessary to develop a guiding technique to confine the laser energy over a long distance (several cm). The interaction can thus take place with a larger volume of plasma resulting in an increase of the extreme ultraviolet (xuv) emission.

Recently, enhancement of the SXRL output has been obtained using two different wave-guiding techniques: the gas-filled capillary discharge waveguide [4] and the hollow dielectric waveguide [5]. In the first case, a few-cm-long capillary is filled with hydrogen and a discharge is triggered inside the tube. A plasma is formed with a parabolic radial electron density profile leading to a guiding structure for the laser pulse. Efficient coupling of the laser beam to the fundamental mode of the waveguide is possible when the waist of the laser spot is properly matched to the plasma channel radius. Such a channel can be doped with xenon, and it was demonstrated that under the optimum conditions for monomode guiding a xuv lasing medium was created along the whole 30 mm of the capillary length with increased energy extraction [6,7]. The second guiding technique employs dielectric capillary tubes in which the laser beam is guided by reflections at the inner wall of the waveguide. Preliminary experiments [8], using 15-mm-long capillary tubes with rough inner surface, have demonstrated the possibility to increase significantly the amplitude of the emitted SXRL.

In this paper we report detailed experimental and theoretical studies of a collisionally pumped OFI SXRL at 41.8 nm driven in capillary tubes with smooth inner surface. An extensive experimental study was conducted in order to understand the key effects related to guiding in this configuration. The plasma was created inside a few-cm-long capillary tubes, and it was shown that maximum xuv emission is obtained when operating in a multimode regime with an optimized lasing signal from a 25-mm-long capillary a factor of

*Present address: Department of X-ray Lasers, Institute of Physics, Na Slovance 2, Prague 8-182 21, Czech Republic.

3 higher than that of a gas cell and with a beam divergence reduced by a factor of 3. As experimental measurements provide time- and space-integrated information on the physical quantities, a numerical modeling was undertaken in order to get some insight into the main physical mechanisms involved and the ways to improve the source further. The modeling of the amplification and of the propagation of the SXRL signal, which is directly connected to the evolution of the population of atomic excited states through collisional-radiative (CR) processes, becomes a formidable task when considering a large volume of amplifying medium, several centimeters long as was achieved in the experiment. Drastic simplifications are thus necessary, while an accurate description of the most important phenomena is required.

The basic features of SXRL generation in a plasma created by OFI of rare gas were first described in Ref. [1], where a high-intensity infrared (ir) beam was used to ionize xenon gas through OFI and generate ions in their ground state. Because the lasing ion Xe^{8+} has a closed subshell, its ionization energy is much higher than the one of Xe^{7+} and it is expected that a large volume of plasma in which the dominant ion is Xe^{8+} will be created. After interaction with the laser beam, ground-state Xe^{8+} ions are excited by electron collisions, which populate the upper level $4d^9 5d\ ^1S_0$ of the lasing line. Inversion of population with the lower level $4d^9 5p\ ^1P_1$ appears mainly because of the difference in degeneracy between the two levels. The 41.8-nm, $4d^9 5d\ ^1S_0 \rightarrow 4d^9 5p\ ^1P_1$ emission can thus be amplified, leading to the SXRL signal. This amplification self-terminates, either because of the reduction of the excitation rate up to the upper level or because there is no more inversion of populations between the upper and lower levels. The latter case occurs at low pressure: because the resonant line is locally absorbed, the population of the lower level is accumulating; the total duration of the x-ray amplification for this case is limited to the lifetime of the upper level, which is about 30 ps. At pressures above 5 mbar, the inverse of the ionization rate becomes smaller than 30 ps, inducing a reduction of the duration of amplification proportional to pressure. Therefore at any pressure the duration of amplification is less than 30 ps. During this short duration the motion of plasma ions is negligible compared to the size of the target. One can therefore neglect hydrodynamic motion and consider a fixed ion density determined from the initial gas pressure. Also due to the short duration of amplification, dynamical effects become important. Only xuv photons propagating in the same direction as the ir pulse and having a group velocity close to the ir one can be amplified over large distances. The emission thus becomes highly directional and moreover the variation of the SXRL group velocity with the gain should be taken into account.

These considerations lead to simplifying assumptions that make possible the calculation of the transport of photons over several centimeters and a direct comparison with experimental results. A numerical code, named COFIXE, was elaborated to calculate the SXRL signal emitted by the plasma source. It includes the calculation of the pump beam propagation, the determination of the plasma state just after the interaction with the pump beam, the calculation of the evolution of the local properties of the plasma during the subsequent few ps, and the calculation of the amplification and transport of the SXRL emission.

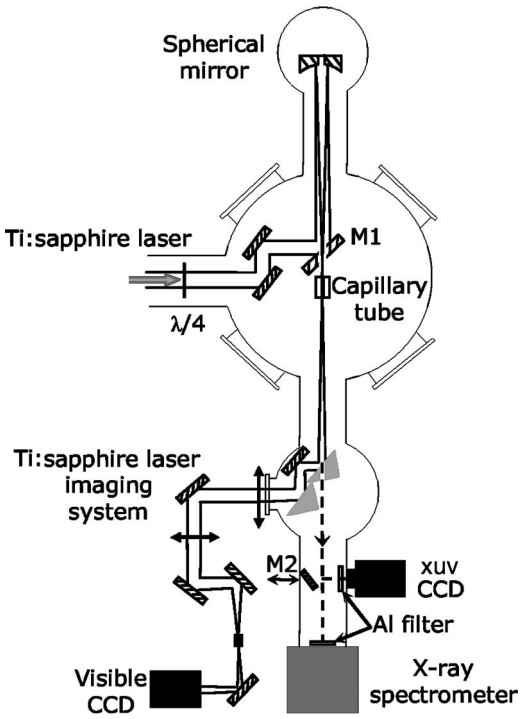

FIG. 1. Experimental setup.

The rest of this paper is organized as follows: in Sec. II experimental results showing the dependence of the SXRL signal with gas pressure and capillary length are presented. In particular, comparison between the characteristics of the xuv beams produced in gas cells and in capillary tubes is emphasized. In Sec. III the main features of the COFIXE code are presented while the results of simulations are presented and discussed with respect to experimental results in Sec. IV.

II. EXPERIMENTAL RESULTS

A. Experimental setup

The experiment was performed at the Laboratoire d'Optique Appliquée with the "Salle Jaune" laser system. This Ti:sapphire laser system with central wavelength 820 nm delivers on target an energy of the order of 1 J per pulse, with pulse duration $\tau \approx 40$ fs full width at half-maximum (FWHM). The experimental setup is shown schematically in Fig. 1. A quarter-wave plate is used after compression to tune the beam polarization. The beam is focused by a 2-m-focal-length ($f/25$), on-axis spherical mirror to a waist (radius at $1/e^2$ in intensity) $w_0 = 25-30\ \mu$m, and a maximum intensity in the range $(0.5-1) \times 10^{18}$ W/cm^2. The capillary tube is mounted on a motorized support with five degrees of freedom (three translations and two rotations) which allow the micropositioning of the entrance plane of the capillary tube in the focal spot plane and of the tube on the laser beam axis. One percent of the transmitted beam is reflected by two successive rejection wedges and sent to optical diagnostics. A $f/10$ doublet images the focal plane or

the output plane of the capillary tube on a 16-bit charge-coupled-device (CCD) camera equipped with a microscope objective, with a resolution of 1 μm per pixel. A hole of 5 mm diameter drilled in the center of the first rejection wedge allows the xuv radiation to pass through and reach the xuv diagnostics. A transmission grating spectrometer located 2 m away from the focal plane is used for the spectral analysis of the emission in the range 0–50 nm, with a resolution of 4.5×10^{-2} nm. A movable, Mo:B_4C:Si-coated, flat mirror with a reflection coefficient of a few percent at 45° for 41.8 nm radiation is placed in the beam path to send the xuv beam to a 16-bit CCD camera for measurements of the far-field pattern. Two 0.25-μm-thick aluminum foils are used to absorb the ir beam.

The glass capillary tubes manufactured by Friedrich & Dimmock have an inner diameter of 305 ± 10 μm, an optically smooth inner surface, and a wall thickness of 2.6 mm. Slits drilled at 3 mm from each end of the tube allow the gas to flow inside the tube. The tube is placed inside a cell filled with gas and vacuum sealed, so that the only gas leaks inside the vacuum chamber occur through the tube holes at each end.

For comparison between guided and unguided cases, the cell was also used without a capillary tube inside: the openings of the cell were then closed with thin glass windows in which pinholes were drilled by the ir laser beam. Tube and cell lengths between 16 mm and 56 mm were used.

B. Properties of the ir beam in the vicinity of the focal plane

An adaptive mirror was used after compression to correct the phase front of the ir laser beam. The correction affects a large region in the vicinity of the best focal plane and induces significant changes as compared to a pure Gaussian beam energy repartition, over several centimeters around the best focal plane along the beam propagation axis. As the maximum intensity achieved in this experiment is more than 10 times higher than the intensity necessary to ionize 8 times the xenon ions, the volume where Xe^{8+} ions are produced should be large and depend on the energy repartition of the ir beam.

The focal spot was measured on high-energy shots and controlled on a regular basis during the experimental run. Figure 2(a) shows a typical image of the ir beam in the focal plane in vacuum, and the corresponding average radial profile is plotted in Fig. 2(b) in plain line and logarithmic scale. The dotted line is a double-Gaussian function which fits the experimental profile closely up to a radius of 60 μm. The first Gaussian is characterized by a waist of 30 μm and contains 28% of the collected energy. Within this approximation, the maximum intensity for this shot is 5.4×10^{17} W/cm^2. The maximum intensity was also estimated by calculating the maximum intensity per pixel: assuming that all the energy delivered in the focal plane is imaged on the CCD chip, the energy per count per pixel can be determined, giving in the present example a maximum intensity of 4.85×10^{17} W/cm^2. Therefore, for this shot, the maximum intensity is estimated to be $(5.1\pm0.3)\times10^{17}$ W/cm^2. For all the data reported in this paper, the maximum intensity, estimated in a similar fashion, was in the range $(5-10)\times10^{17}$ W/cm^2.

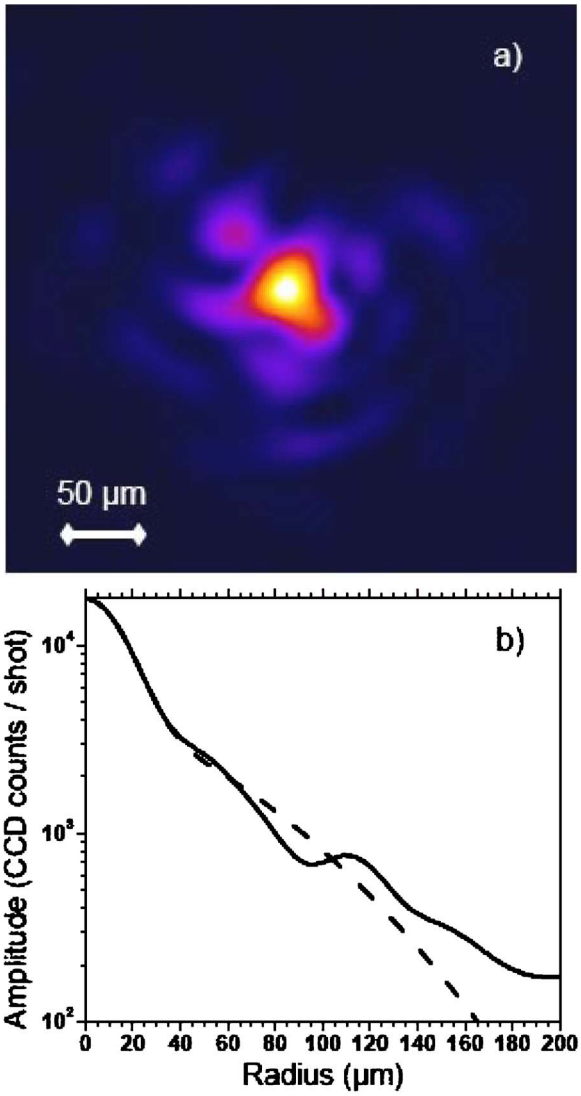

FIG. 2. (Color online): (a) Image of the ir intensity in the focal plane measured in vacuum and (b) corresponding average radial profile (solid line) and double-Gaussian fit (dotted line).

The intensity repartition was also measured in different planes in the vicinity of the best focal plane: up to 1 cm away from the best focal plane, the beam radius containing up to 50% of the energy expands like a Gaussian beam with an associated Rayleigh length $z_R\sim3$ mm; farther away, the beam becomes annular.

C. Characterization of SXRL signal

In order to evaluate the effect of guiding on the observed SXRL signal, the same types of measurements have been performed with and without a waveguide by using a gas cell of the same length as the capillary tube.

1. Observation of the SXRL

The SXRL signal at the output of a gas cell was measured as a function of the polarization of the incident ir laser by

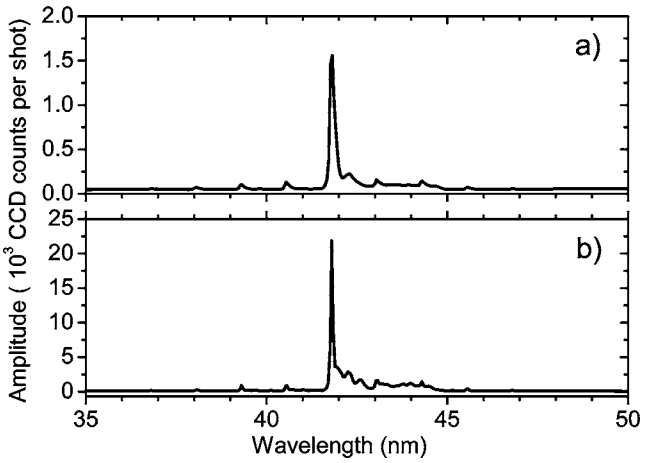

FIG. 3. Single-shot spectrum in the X-uv range for a xenon pressure of 11 mbar, at the output of (a) a 25-mm-long gas cell and (b) a 25-mm-long capillary tube.

rotating the quarter-wave plate. It was checked that the maximum SXRL signal at the output of capillary tubes was obtained for the same position of the quarter-wave plate that gave the optimum signal for the gas cell.

The amplitude of the SXRL signal was found to exhibit a maximum when the position of the focal plane of the ir beam in vacuum was located after the entrance plane of the target. In the conditions of the experiment, the optimum distance between the entrance plane of the target and the focal plane was 8 mm for the gas cells and 3 mm for the capillary tubes.

Figure 3 shows single shot spectra recorded for a xenon pressure of 11 mbar, with a 25-mm-long gas cell [Fig. 3(a)] and with a 25-mm-long capillary tube [Fig. 3(b)]. It is seen that for both the gas cell and the capillary tube strong lasing occurred at 41.8 nm, the SXRL signal dominating the 50 -nm bandwidth of the recorded spectra. The signal recorded at 11 mbar with the capillary tube was approximately 14.5 times larger than that achieved with the gas cell at the same filling pressure. The small-amplitude, regularly spaced peaks on each side of the SXRL peaks arise from diffraction of the beam by a mesh supporting the grating.

2. Pressure dependence

The SXRL signal was measured as a function of the xenon filling pressure and is displayed in Fig. 4 for a 16-mm-long gas cell (squares), a 16-mm-long capillary tube (dots), a 25-mm-long tube (open circles), and a 30-mm-long tube (triangles). The lines are a guide to the eye; each point is the average value of three different shots and the error bars include the standard deviation from shot to shot as well as spatial variation of the amplitude along the beam transverse profile.

The xuv radiation generated inside capillary tubes exhibits a maximum amplitude in the pressure range 10–15 mbar, whereas inside a cell the maximum amplitude occurs for higher pressure, here 25 mbar for a 16-mm-long cell. The same pressure dependence, although not shown in the figure, was also observed for capillary tubes up to 56 mm long.

3. Length dependence

Figure 5 shows the amplitude of the SXRL signal as a function of the target length for capillary tubes (dots) and for

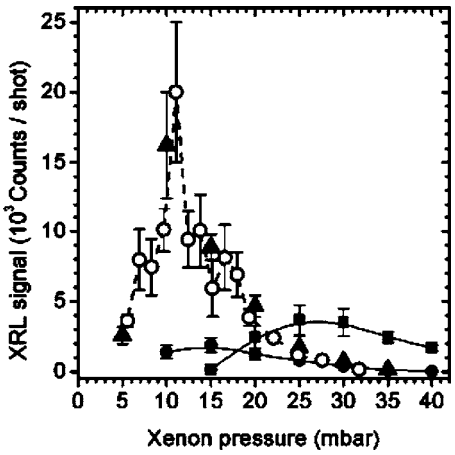

FIG. 4. Experimental results for the SXRL amplitude as a function of xenon filling pressure at the output of a 16-mm-long cell (squares), a 16-mm-long capillary tube (dots), a 30-mm-long capillary tube (triangles), and a 25-mm-long capillary tube (open circles).

gas cells (squares) for xenon filling pressure corresponding to the optimum for each case—i.e., 10–15 mbar for capillary tubes and 25 mbar for gas cells. The dotted lines are a guide to the eye, while the solid (dashed) line is the result for the cell (capillary tube) case of simulations with the COFIXE code described in Sec. III. A cell with tunable length was used, allowing a fine variation of the cell length from 1 to 21 mm.

Figures 4 and 5 show that the maximum SXRL signal occurs at the output of the 25-mm-long capillary tube for a pressure of 11 mbar at which it is about 75 times higher than the output of a 25-mm-long cell. The capillary tube output remains large in the range of length studied, with a maximum for capillary tubes of length 25–30 mm. The amplitude is divided by 2 when the length is increased from 25 to 56 mm. The fast growth for small cell lengths is expo-

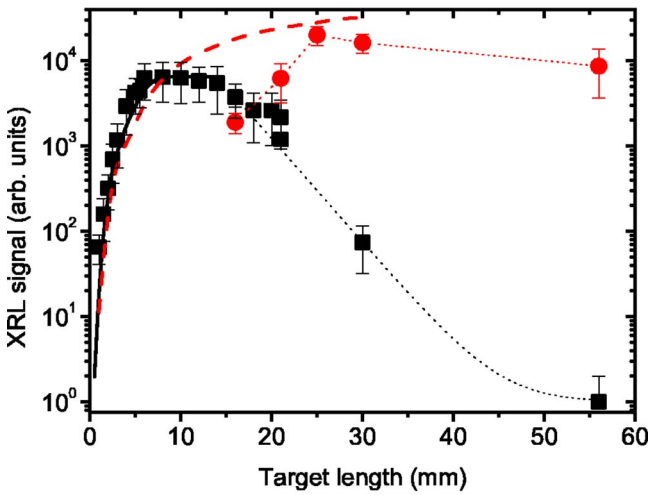

FIG. 5. (Color online) Amplitude of the SXRL signal as a function of the target length; experimental results for cells with a xenon filling pressure of 25 mbar (squares) and capillary tubes at 10 mbar (dots); theoretical calculations for gas cells (solid line) and capillary tubes (dashed line).

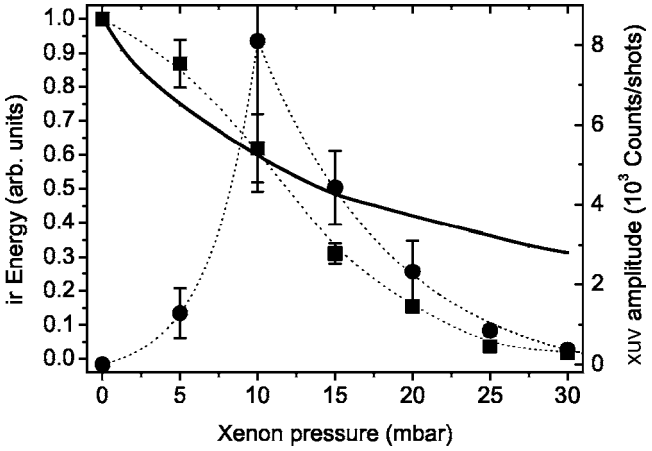

FIG. 6. Experimental results for the transmission of the ir beam (squares) and the SXRL output (dots) as a function of xenon filling pressure; theoretical result (solid line) for the transmission of the ir beam, considering cold, nonionized, wall.

nential and is fitted by e^{GL} with $G=28\pm2$ cm^{-1} and L is the cell length; then the SXRL output saturates and reaches a plateau followed by an exponential decay fitted by $e^{-\alpha(\text{L-13.4})}$ with $\alpha=2.8$ cm^{-1}.

The optimized signal at the output of the 25-mm capillary tube is 3 times higher than at the output of a 8-mm cell filled with 25 mbar of xenon, which are the conditions in which the SXRL amplitude was maximum in the unguided case. When the length of either the tube or the gas cell is further increased beyond 30 mm for the tube and 16 mm for the cell, the SXRL signal decreases quickly denoting strong absorption of the 41.8-nm line in Xe plasma, when the average charge of the Xe atoms becomes much lower than 8.

4. Correlation between guiding and SXRL emission

In order to understand the importance of the conditions of propagation of the ir beam on the generation of xuv radiation, the properties of the ir beam were measured in vacuum and in the presence of xenon.

The transmission of the ir beam and its relation to the SXRL emission were studied in detail for the 30-mm-long capillary tube. The hole drilled in the first wedge of the ir imaging system (see Fig. 1) allowed one to measure in the same shot part of the SXRL output going through the hole and the reflected ir output. The ir beam was then collected and imaged on the CCD camera. The ir beam energy (squares), normalized to its maximum, and the SXRL (dots) at the output of the capillary tube are plotted in Fig. 6 as a function of xenon filling pressure; dotted lines are a guide to the eye and the solid line is the simulation result for the ir transmission assuming cold, nonionized glass walls. The transmission of the ir beam in vacuum is high, of the order of 90%–95% of the input energy. As the xenon pressure is increased, the transmitted ir energy drops slowly to 60%, then much faster for pressures larger than 10 mbar. The SXRL output quickly grows with pressure up to 10 mbar, where it reaches a maximum; then it decreases more slowly. The maximum of the X-uv output occurs for a pressure value for which the ir transmission is still high; for pressures higher than 10 mbar the SXRL output decrease is similar to the ir transmission one. Due to the strong decrease of guiding efficiency with pressure above 10 mbar, the optimum pressure value in the capillary is much lower than in the gas cell, as observed in Fig. 4.

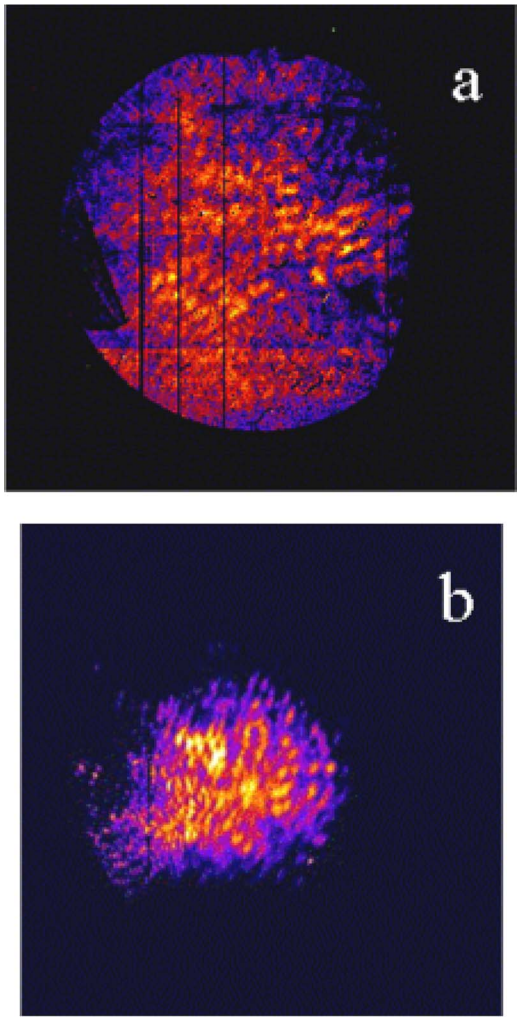

FIG. 7. (Color online) Far-field pattern of the SXRL laser beam at the output of (a) a 8-mm-long cell for a xenon pressure of 25 mbar and (b) a 25-mm-long capillary for a pressure of 11 mbar.

5. Far-field pattern

Figure 7 shows the single-shot, far-field pattern of the SXRL beam recorded at the output of a 8-mm-long cell for a xenon pressure of 25 mbar [Fig. 7(a)] and at the output of a 25-mm-long capillary for a pressure of 11 mbar [Fig. 7(b)]. The main feature is that the divergence of the beam is reduced to about 5.5 mrad at the output of the capillary tube while it is of the order of 12.5 mrad at the output of the cell. Both patterns exhibit a small-scale structure similar to what is observed in laser-produced speckle patterns [9]. As pointed out in Ref. [10] the presence of speckle indicates that the SXRL source has a high longitudinal (temporal) coherence but a low transverse (spatial) coherence.

III. DESCRIPTION OF THE CODE COFIXE

A realistic calculation of the SXRL signal emitted by the plasma source should include three major contributions: the determination of the plasma state just after interaction with the ir beam, the evolution of the local properties of the plasma during the subsequent few ps when the amplification takes place, and the transport of the SXRL. To perform these calculations, we have constructed a numerical code named COFIXE.

A. Main assumptions

As we are considering several-centimeter-long targets, drastic simplifications are necessary to obtain final results using a reasonable amount of computing resources, while accuracy requires that the most important phenomena are correctly taken into account. In COFIXE, a two-dimensional (2D) axis symmetry around the laser-beam propagation axis is assumed. The most demanding task, in terms of computer resources, is the calculation of the atomic dynamics in the 2D space. In COFIXE, this calculation has been dramatically simplified by assuming that the evolution with time of the plasma properties at one point inside the target depends only on the maximum intensity of the ir beam at the considered position. It allows transforming the 2D mapping to a 1D one, which can be parametrized without much effort. This transformation is justified by the following remarks.

(i) In the considered range of gas pressure, between 5 and 30 mbar, the ir pulse duration ($\sim$40 fs) is much smaller than any characteristic time related to the relaxation through collisions either of the electron distribution function or of the atomic-state populations. Therefore the collisional-radiative equations are solved without direct interaction with the laser beam.

(ii) The influence of the transport of particles and photons is neglected in the CR equations, with the consequence that these equations can be solved locally. Characteristic times for the transport of particles are much longer than the duration of the SXRL amplification process. For photons, the influence of transport, from highly ionized zones to less ionized ones, is more difficult to estimate. Photons, with a relatively large mean free path, can have a non-negligible contribution by providing additional mechanisms for excitation and ionization of lower ionization states such as Xe^{6+} and Xe^{7+}. This mechanism can be beneficial for enlarging the Xe^{8+} domain around the axis. The dimension of the amplifying plasma will thus be slightly underestimated by the simulation. The CR equations being local, the time dependence at each spatial point can be expressed using the variable $\tau = t - z/v_{ir} \simeq t - z/c$, z being the longitudinal coordinate and v_{ir} the group velocity of the ir beam, which in our experimental conditions is very close to the speed of light in vacuum.

(iii) Due to the short duration of the ir pulse, the state of the plasma just after interaction with the ir laser, in particular the distribution of charge and the velocity distribution function of the free electrons, depends only on the OFI process; all other collision processes, such as inverse-bremsstrahlung heating, can be safely neglected. Moreover, as ionization through OFI is a rather fast process compared to the variation of the ir amplitude, one can assume that the state of the plasma just after the passage of the ir laser pulse only depends on the maximum of the ir intensity at the considered point, which will be labeled $I_{\max}(r,z)$, r being the radial coordinate. It allows us to write all local physical parameters as a function only of $I_{\max}(r,z)$ and of the local time τ.

Within the above approximations the determination of the SXRL emitted by a gas target irradiated by an ir pulse can be done by COFIXE through three successive independent calculations which are described below.

B. Transport of the ir beam

The calculation of the transport of the ir beam is used to determine tables of $I_{\max}(r,z)$ on a grid in (r,z) for further use as input data to the CR code. The transport of the ir beam is closely connected to the OFI process. As the ir beam propagates inside the gas, xenon atoms become more and more ionized; as the ionization probability strongly depends on the intensity of the laser, the ir beam will interact with a plasma that is inhomogeneous both in longitudinal and in transverse directions. For the considered range of pressure, the energy lost in ionizing the atoms is small and can be neglected. Moreover, the beam intensity inside the plasma being well below 10^{18} W/cm^2, nonlinear relativistic effects can also be neglected.

Within COFIXE, the transport of the ir beam inside xenon gas is calculated within the paraxial approximation in a 2D-axis symmetry geometry [11]:

$$2ik_0\frac{\partial a(r,z,\tau)}{\partial z} - \frac{2}{c}\frac{\partial^2 a(r,z,\tau)}{\partial \tau \partial z} + \Delta_\perp a(r,z,\tau) = k_0^2\frac{n(r,z,\tau)}{n_c\gamma}a(r,z,\tau), \quad (1)$$

where $k_0 = 2\pi/\lambda_0$, $a(r,z,\tau)$ is the scalar amplitude of the electric field of the ir beam, $\Delta_\perp = r^{-1}\partial/\partial r(r\partial/\partial r)$ is the transverse part of the Laplace operator, $n(r,z,\tau)$ is the free electron density, $n_c = \pi mc^2/(\lambda_0^2 e^2)$ is the critical density at λ_0, m and e being the mass and charge of the electron, and γ is the relativistic factor, which, in the considered intensity range, is close to 1. In front of the ir pulse, $n(r,z,\tau)$ is increasing with time due to sequential ionizations of the xenon atoms, but at the considered pressures, it remains much smaller than n_c. For intensities in the range 10^{16}–10^{17} W/cm^2, the ionization rate can be calculated within the tunnel approximation; the semiclassical Ammonosov-Delone-Krainov (ADK) formula [12] was used to calculate the ionization probability. Using this probability, the energy distribution function (EDF) of ionized electrons has been calculated following the work of Pert [13]. This EDF strongly depends on the polarization of the ir beam, circular polarization yielding electrons with much higher energies. A typical value for the average energy of the electrons after ionization of xenon atoms up to Xe^{8+} is 350 eV using circular polarization, whereas it is less than 100 eV with linear polarization. The upper level of the 41.8-nm lasing line having an excitation energy of 104 eV, the pumping rate of this level is much higher with circular polarization, which leads to the strongest SXRL signal, as it

was observed experimentally [2]. All the simulation results presented here have been obtained using a circularly polarized ir beam.

C. Local evolution of the amplifying plasma: CR model

The local evolution of the properties of the plasma has to be determined in order to calculate the time dependence of the parameters that contribute to SXRL amplification. The plasma generated by OFI will evolve mainly because of electron-ion and electron-electron collisions. On a short time scale, electron-ion collisions excite the lasing ions and populate excited states, such as the upper and lower lasing levels. Ionization of lasing ions by electron-ion collisions will induce a self-termination of SXRL amplification. Electron-electron collisions make the EDF relax to a Maxwellian EDF. The initial EDF is far from a Maxwell distribution; in particular each ionization process $X^{q+} \rightarrow X^{(q+1)+}$ yields a bunch of electrons with energies peaked around a value which increases quickly with q. Therefore, the relaxation time being comparable with the inverse of the ionization rate, nonequilibrium effects should be considered for the calculation of electron collision cross sections. In order to obtain the most accurate results for the variation of the local properties of the plasma we have combined the newly obtained experimental values for the variation with time of the local gain [14] with theoretical calculations, which are still needed to calibrate experimental results. Our theoretical calculations follow closely the work of Pert [15,16], in which the evolution of the atomic populations is calculated in parallel with the relaxation of the EDF determined by solving a Fokker-Planck equation. For the atomic data we have considered 128 levels of Xe^{8+}, whose properties were calculated by the SUPERSTRUCTURE [17] atomic code, while the collision strengths were determined from the related distorted-wave code [18]. A crude approximation is used for the photons emitted by radiative decay. Resonant radiation to the ground level has a very small mean free path and is thus absorbed locally, while for transitions between two excited levels, the photons have a much larger mean free path and can escape freely. This emission of photons induces a cooling of the plasma electrons, which, in our case, was no more than 10% during SXRL amplification.

The local evolution of the plasma parameters, leading to the variation of the amplifying properties for the SXRL, has been determined for several values of $I_{\max}$. From these calculations the local plasma properties were written for the full range of $I_{\max}$ as interpolating parametric formula. As detailed in [14], the time variation contained in these formula was then slightly changed in order to best reproduce the experimental results of Ref. [14].

D. SXRL transport and amplification

Let $I(r,z,\lambda,\Omega,t)$ represent the intensity per unit of wavelength and per steradian of the SXRL signal at the position (r,z), wavelength λ, time t, and in the direction Ω. By extending the work of Ref. [19] to 2D geometry and including the angular dependence of the SXRL intensity, $I(r,z,\lambda,\Omega,t)$ is found to satisfy the propagation equation

$$\left(\frac{1}{v_X(r,z,t)}\frac{\partial}{\partial t}+\frac{\partial}{\partial s}\right)I(r,z,\lambda,\Omega,t) = G(r,z,\lambda,t)I(r,z,\lambda,\Omega,t)+E(r,z,\lambda,t), \quad (2)$$

where $v_X(z,r,t)$ and s are the local group velocity of the SXRL signal and the distance traveled along the direction Ω, $G(r,z,\lambda,t)$ is the local gain, and $E(r,z,\lambda,t)$ is the source term due to spontaneous emission. The considered plasma conditions are similar to the ones considered in Refs. [18,20], in particular concerning the validity of the quasi-steady-state approximation (QSSA). In the QSSA it is assumed that the ratio between the populations of the upper and lower levels of the lasing line for the frozen charge state has a relaxation rate much larger than the one related to ionization of the ground level. The results of the CR code confirm that the QSSA is indeed valid for the 41.8-nm line of Xe^{8+}. Following [19,20] the saturation of the gain and of the spontaneous emission can then be introduced through the relations

$$G(r,z,\lambda,t)=\frac{f(r,z,\lambda,t)g(r,z,t)}{f(r,z,0,t)[1+I_{av}(r,z,t)/I_s(r,z,t)]} \quad (3)$$

and

$$E(r,z,\lambda,t)=\frac{f(r,z,\lambda,t)e(r,z,t)}{4\pi[1+I_{av}(r,z,t)/I_s(r,z,t)]}, \quad (4)$$

where g and e are, respectively, the small signal gain and the small signal emissivity at the line center, $f(r,z,\lambda,t)$ is the normalized line profile (assumed to be identical for stimulated and spontaneous emission), I_s is the saturated intensity, and I_{av} is the average intensity, $I_{av}(r,z,t)=\int I(r,z,\lambda,\Omega,t)f(r,z,\lambda,t)d\lambda d\Omega/f(r,z,0,t)$.

The group velocity entering Eq. (2) is given by [19]

$$v_X(r,z,t)=\frac{c}{1+\dfrac{\lambda_c^2 G(r,z,\lambda_c,t)}{\Delta\lambda(r,z,t)}}, \quad (5)$$

λ_c being the center wavelength of the lasing line and $\Delta\lambda(r,z,t)$ the width (FWHM) of $f(r,z,\lambda,t)$. Due to the large mass of Xe atoms and to the high average energy of electrons, the electron-ion coupling through binary elastic collisions is ineffective for heating ions during the SXRL amplification. Collective effects between ions can heat the ions through relaxation of potential energy into kinetic energy, leading to an ion temperature after relaxation of few eV [21]. Therefore, at pressures above 5 mbar, Doppler broadening remains smaller than collisional broadening, and $f(r,z,\lambda,t)$ is thus written as a Lorentzian function of λ.

From the results of the CR calculations, the parameters of Eqs. (2)–(5) are written as functions of τ with $I_{\max}(r,z)$ as a parameter, $g(r,z,\tau)=g_{I_{\max}(r,z)}(\tau)$; similar expressions for the other physical quantities are obtained. Recently, an ultrashort x-ray pulse generated by a high-order harmonics source was injected into an amplifying plasma created by OFI and was used to determine experimentally the evolution with time of the local gain [14]. In the present work we use theoretical values for the maximum of the gain and of the emissivity,

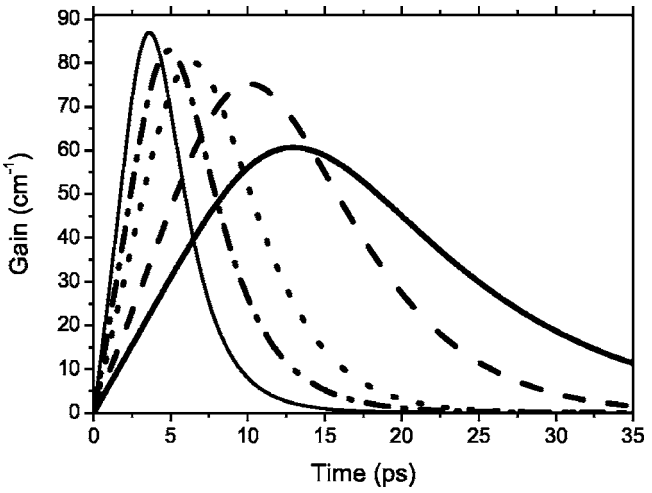

FIG. 8. Evolution with time of the small signal gain as used in the simulation, at a xenon pressure of 6.7 mbar (thick solid line), 13.3 mbar (dashed line), 20 mbar (dotted line), 26.7 mbar (dot-dashed line), and 33.3 mbar (thin solid line).

while their time variation is deduced from the results of the experiment reported in Ref. [14]. For $g_{I_{\max}}(\tau)$, we thus use a dependence of the form

$$g_{I_{\max}}(\tau) = g_1 \tau \exp[-\tau(g_2 + \tau g_3)]/(1 + g_2 \tau^2), \qquad (6)$$

g_1, g_2, and g_3 being functions of $I_{\max}$; a similar form has been used for $E_{I_{\max}}(\tau)$. I_S, having a relatively small variation, was taken as a linear decreasing function of τ.

The calculated small signal gain is plotted in Fig. 8 as a function of time for a xenon pressure of 6.7 mbar (thick solid line), 13.3 mbar (dashed line), 20 mbar (dotted line), 26.7 mbar (dot-dashed line), and 33.3 mbar (thin solid line). This figure shows that the duration of the SXRL amplification is inversely proportional to gas pressure. Simulations and the experiment reported in Ref. [14] are in good agreement to find that this duration is due to ionization of Xe^{8+}.

Using parametrized forms and the table of $I_{\max}(r,z)$ provided by the resolution of the TR-ir equation, Eqs. (2)–(5) can be integrated to determine the SXRL output energy. The evolution with time of the x-ray intensity was calculated on a grid in (r,z,λ,Ω), and typical values for the size of the grid were (30,2000,10,30) with a corresponding running time of 1–3 days on one processor of our PC cluster.

IV. SIMULATION RESULTS AND DISCUSSION

The COFIXE code has been used with the parameters of the experiment presented in Sec. II for the case of the cell and of the capillary tube. The ir laser pulse, circularly polarized and with central wavelength 820 nm, has a maximum intensity in vacuum of 5.1×10^{17} W/cm^2 and a radial profile in the focal plane given by the double-Gaussian function plotted in Fig. 2(b). Its pulse duration (FWHM) is 40 fs. The focal planes are chosen at the experimentally observed optimum positions: at 8 mm from the gas cell entrance and at 3 mm from the capillary one. For the capillary specific conditions are required to take into account the boundaries at the entrance of the tube and the reflection from the walls during the propagation inside the tube.

A. Boundary conditions

Equation (1) has been solved using the incoming beam in free space as a boundary condition in the plane $z=0$, corresponding to the entrance of the target. Following the experimental intensity profile, an example of which is given in Fig. 2(b), the injected ir beam is described as the sum of two Gaussian modes, one with a waist of 30 μm and the second one with a waist of 117 μm. When considering guiding inside capillary tubes, the following boundary condition at the wall $r=r_0$ has been used [11]:

$$\left[\frac{\partial a(r,z,\tau)}{\partial r}\right]_{r=r_0} = ik_{w\perp}\left(1 + \frac{i}{k_0 c}\frac{\partial}{\partial \tau}\right)a(r_0,z,\tau),$$

$$k_{w\perp} = \frac{2(\varepsilon_w - 1)^{1/2}}{\varepsilon_w + 1}, \qquad (7)$$

where ε_w is the dielectric constant of the wall. For a radial flux of the ir beam at the wall below ionization threshold, one can use the cold value of the dielectric constant of SiO_2, $\varepsilon_w = 2.25$. As seen in Fig. 6, a calculation (solid line) performed with this value of ε_w gives results in good agreement with experimental results (squares) for the transmission of an ir beam through a 3-cm-long capillary, for pressure values up to 10 mbar.

The intensity of the ir beam is higher on axis, so that the ionization state of Xe ions and the electron density are decreasing functions of r. Therefore the dielectric constant of the target plasma, $\varepsilon_P = 1 - n/n_c$, is an increasing function of r. This gradient of ε_P induces a radial deflection of the ir beam away from the axis and thus increases the transverse flux at the wall. At pressures higher than a few mbar, this deflection can become large enough for the intensity of the transverse flux to reach the threshold for plasma creation at the capillary wall. From the comparison of experimental results and calculation in the case of a cold wall plotted in Fig. 6, we infer that it occurs at pressures above 10 mbar. To take this effect into account we have introduced in the simulation, at pressures above 10 mbar, a pressure-dependent value of ε_w in order to reproduce the experimental values of Fig. 6 for the transmitted ir energy at all pressures.

B. Maps of ionization states

The solution of Eq. (1) gives the map of maximum intensity $I_{\max}(r,z)$ from which the charge state map is calculated. In Fig. 9 are plotted the isocontours of the average charge state of xenon ions obtained by solving Eq. (1) for the case of a target cell at 25 mbar [Fig. 9(a)] and for a capillary tube at 10 mbar [Fig. 9(b)]. Four regions can be distinguished in these figures.

The first region (white area), with ionization state above 8, corresponds to maximum intensities above 8×10^{16} W/cm^2. As recombination rates are too small for the recombination process to play a role during the few ps of

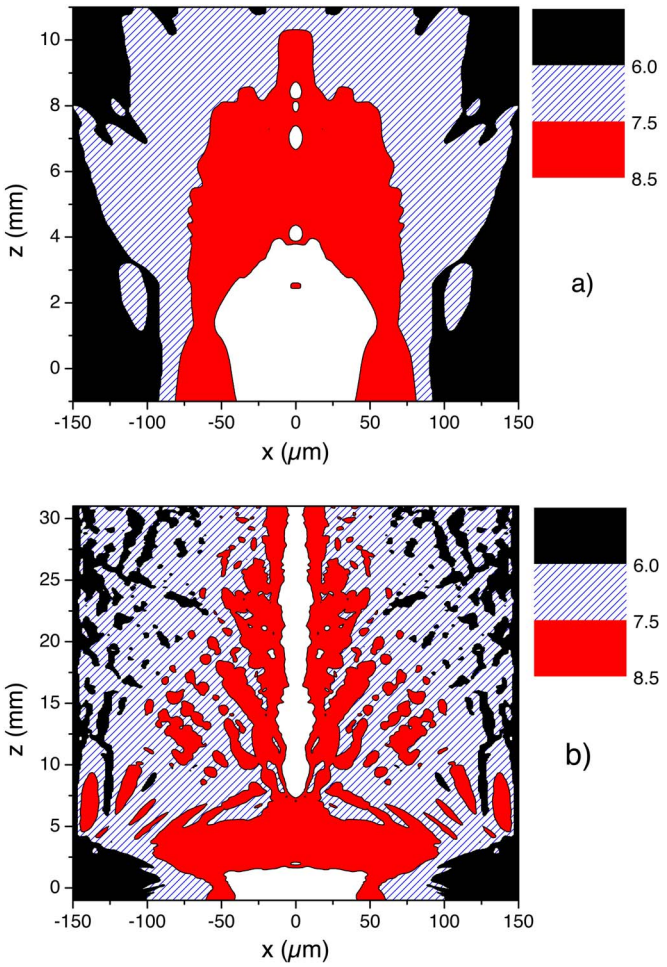

FIG. 9. (Color online) 2D map of the simulated average ionization state of a xenon plasma created by OFI (a) in a 10-mm-long cell and (b) in a 3-cm-long capillary tube of 150 μm radius. At both ends of the targets ($z<0$ and $z>10$) there is a 1-mm zone that accounts for gas leakage outside the target.

SXRL amplification, this region cannot contribute to the SXRL signal. The size of the overionized region depends on the position $z=z_F$ of the focal plane of the ir beam in vacuum. By increasing the value of z_F, the ir intensity at the entrance of the target, $z=0$, can be reduced as well as the size of the over overionized region. However, for too large values of z_F, the length of the Xe^{8+} region starts to decrease because of the divergence induced by the density gradient. A maximum SXRL energy is thus obtained for an optimized value of z_F as was observed already in previous experiments [8]. The results shown in Fig. 9 have been calculated for the experimentally observed optimal values of $z_F=8$ mm for the gas cell and $z_F=3$ mm for the capillary. In the capillary case, for higher values of z_F, the entrance hole reduces the injected energy and furthermore induces diffraction that increases the transverse flux at the wall, thus decreasing the transmitted ir energy through the tube. The simulation predicts a rather large overionized region that can be observed for the capillary close to the z axis along the whole target length. A perfect axis symmetry of the laser beam is assumed in the simulation; a deviation from this symmetry will reduce the intensity along the z axis.

The second region (grey-red area) in Fig. 9 corresponds to maximum intensities between 1.8×10^{16} and 8×10^{16} W/cm^2. For this range of intensities, the dominant ionization state created by OFI is Xe^{8+}. This region can contribute to SXRL emission by direct pumping from the ground level up to the upper lasing line through electron collisions. The third region in which OFI produces mainly Xe^{6+} and Xe^{7+} is the dashed area in Fig. 9. These two ions can contribute to SXRL emission only in case of further ionization and excitation, through collisions by electrons or absorption of photons, in a sufficiently short time. In the present state of the atomic code, only the ground state of ions other than the lasing ion is included and excitations through radiative transfer are not considered. Therefore, in the simulation, the Xe^{6+} and Xe^{7+} regions have only a small contribution to SXRL. Nevertheless, an analysis of recent experimental data of the amplification of an injected high-order harmonic beam [14,22] has shown that the Xe^{6+} and Xe^{7+} regions can have a non-negligible contribution. The theoretical gain has been adjusted as described by Eq. (6) to fit the experimental results of [14]. The last region (black area) in Fig. 9 corresponds to the lowest-charged ions, which do not participate to the amplification of the SXRL signal, but instead can absorb x-ray photons, leading to a reduction of the SXRL signal.

Figure 9 shows that SXRL amplification can occur over several mm in the gas cell and over the full, 3 cm length of the capillary tube. In the latter case the effect of reflection on the walls is clearly seen. The radius of the amplifying plasma is in the range of 50–100 μm both in the cell and in the capillary tube.

C. Amplitude of SXRL

The results obtained by the COFIXE code by combining the calculations of the transport of the ir beam with Eqs. (2)–(5) are shown in Fig. 10: the SXRL energy emitted by the plasma source, for the gas cell [Fig. 10(a)] and the capillary tube [Fig. 10(b)], is plotted as a function of the target length for different xenon pressures indicated by labels on the curves. All the curves exhibit common features: an exponential growth for target lengths of the order of a few millimeters, followed by linear growth and saturation.

The exponential growth of the signal for short target lengths is associated with fast modifications in the x-ray signal characteristics, such as a small group velocity and a gain narrowing of the linewidth and of the signal duration.

Calculations show that the SXRL intensity becomes close to I_S after a few millimeters of amplification. As can be seen in Fig. 10, for target lengths above a few mm, the energy of the SXRL signal increases nearly linearly with the length of the target, indicating that amplification has reached the saturated regime for which $I_{av}(r,z,t)>I_S(r,z,t)$. In this regime, taking $1+I_{av}(r,z,t)/I_S(r,z,t)\simeq I_{av}(r,z,t)/I_S(r,z,t)$ in Eq. (3) and integrating Eq. (2) over λ and Ω, one gets

$$\left(\frac{\partial}{\partial z}\right)I_{av}(r,z,\tau)\approx g(r,z,\tau)I_S(r,z,\tau). \tag{8}$$

The SXRL average intensity thus increases with z as the amplifying plasma volume. Considering the SXRL energy, a

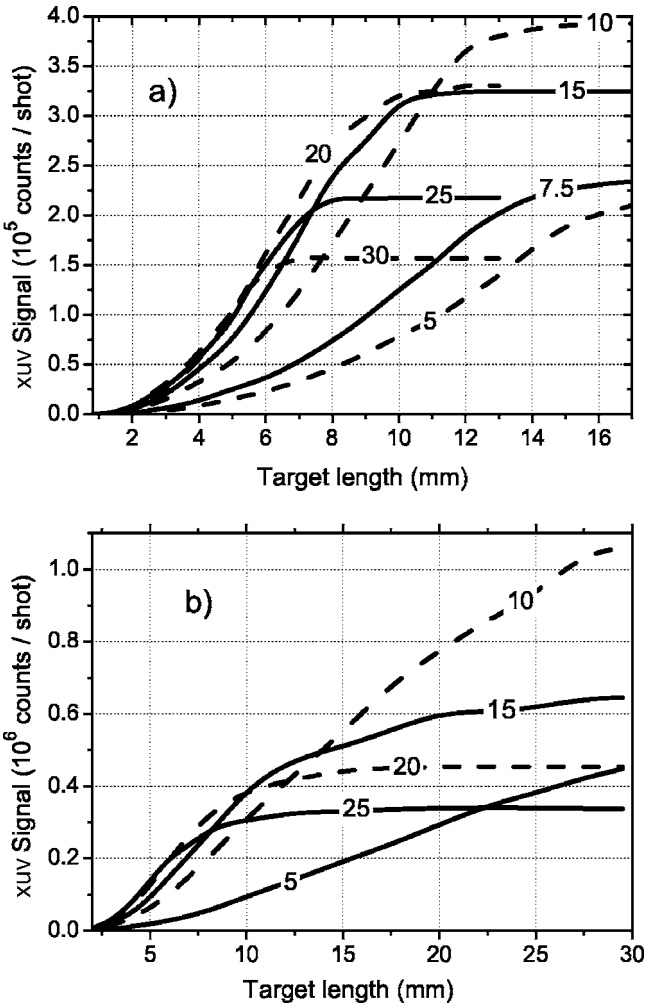

FIG. 10. Simulation results for the energy of the SXRL signal as a function of target length for (a) a gas cell and (b) a capillary tube. The label on each curve indicates the value of xenon pressure in mbar.

small additional factor is the duration of the signal, which increases slightly with the target length due to a variation of the group velocity at the rear side of the signal [3]. SXRL durations (FWHM) of 4.5 ps for a 8-mm gas cell at 25 mbar and of 14 ps for a 3-cm capillary tube at 10 mbar are obtained from simulations. The ratio between these two durations is 3, slightly more than the pressure ratio (2.5); the difference between these two ratios can be attributed to dispersion effects. The almost linear increase of the SXRL signal finally stops when there is no more amplifying plasma; due to the defocusing induced by the density gradient of free electrons the growth stops for smaller propagation lengths when the pressure is increased. As seen in Fig. 10, the almost linear regime is more apparent at low pressures and when guiding is used [Fig. 10(b)]. This regime of guiding is more effective at low pressures, for which the plasma length inside the capillary is increased by more than a factor of 2 compared to the gas cell.

Equation (8) shows that in the saturated regime, the SXRL energy E_{SXRL} scales as $E_{\mathrm{SXRL}} \propto I_S V_P \Delta\tau$, where V_P is the amplifying plasma volume and $\Delta\tau$ is the duration of the SXRL pulse. $\Delta\tau$ is inversely proportional to gas pressure, while I_S increases more than linearly with pressure. Thus, for a given value of V_P, E_{SXRL} should increase with pressure. This is observed in Fig. 10: for target lengths shorter than 7 mm, the highest signal is obtained at the highest pressures. For longer targets, the influence of the target pressure on V_P plays a more dominant role, the maximum for E_{SXRL} being obtained at lower pressures.

D. Comparison between experiment and simulation

1. Length dependence

Simulation results for the variation of the SXRL signal with target length are plotted as solid and dashed lines in Fig. 5 for comparison with experimental results. The simulation data have been scaled so as to reproduce the maximum value of the experimental signal for the gas cell, achieved for a length of 8 mm. The simulation curve fits perfectly the experimental data for the gas cell, describing the same exponential growth up to saturation. As can be seen in Figs. 9(a) and 10(a), simulation predicts an amplifying plasma length of 8 mm in the gas cell at 25 mbar, in good agreement with the experimental results of Fig. 5.

The effect of absorption, presently not included in the simulation, is clearly seen on the experimental curves of Fig. 5; it can be used to determine the length beyond which the ionization state of xenon ions remains smaller than 8 during the SXRL emission. In the case of the gas cell, the experimental curve for target lengths above 8 mm exhibits two different decay slopes. The first one, for target lengths smaller than 15 mm, corresponds to an attenuation length of 30 mm, while for longer targets, the attenuation length comes close to 3.5 mm. The latter value is comparable to the attenuation length of neutral xenon gas at 25 mbar equal to 2 mm according to Ref. [23]. The 32.6-eV x-ray lasing line can be absorbed mainly through bound-free transitions, which for highly ionized Xe are possible only from excited states, yielding a large attenuation length. A large increase of the absorption cross section is expected when the binding energy of the ion ground state is smaller than 32.6 eV; for Xe, it occurs for charge states lower than 3. The simulations of propagation show that at 25 mbar, the average ionization state around the z axis is above 3 up to a length of 15 mm, in good agreement with Fig. 5.

In the capillary case the reduction of the signal at 56 mm compared to the amplitude at 30 mm corresponds to an attenuation length of 38 mm, to be compared with the attenuation length of 5 mm for 10 mbar of neutral xenon gas. It indicates that, due to the guiding of the ir beam, the plasma remains highly ionized nearly up to the largest target length.

Comparing in Fig. 5 the maximum signal obtained in the capillary and in the gas cell, the simulation yields an enhancement factor of 4.8 due to guiding, whereas the experiment gives a factor of 3, the difference between the two values being within the error bars. The maximum difference between simulation and experimental results occurs in the capillary case for target lengths equal to 16 and 21 mm, where the experimental data are well below the simulation curve. One possible explanation is that at short lengths, the

plasma created by the ir beam is more sensitive to focusing conditions at the capillary entrance. In particular the diffraction of the laser beam at the capillary walls can have a significant influence on the plasma nonuniformity close to the capillary entrance. It appears also that the same discrepancy occurs for a gas cell at low pressures (see below).

2. Far-field pattern

The far-field pattern (cf. Fig. 7) gives information on nearly the full x-ray energy emitted by the plasma source. The strong enhancement of the beam quality observed in the experiment is well reproduced by the simulation which yields 17 mrad for the cell and 4.6 mrad for the capillary tube, to be compared with 12.5 mrad and 5.5 mrad values given by the experiment. After averaging over the small structure of Fig. 7, the maximum intensity was found to be 8 times larger with the capillary than with the cell, in good agreement with the simulation that predicts an enhancement of a factor of 10 due to guiding. The COFIXE code predicts that the total energy emitted by the capillary and the cell is 10 μJ and 5 μJ, respectively.

3. Pressure dependence

The simulation results for the variation of the SXRL signal as a function of target pressure are plotted in Fig. 11 for (a) gas cells of length 4 mm (open circles), 8 mm (open triangles), and 16 mm (open squares) and (b) capillary tubes of lengths 16 mm (open squares), 25 mm (open triangles), and 30 mm (stars), together with some experimental results already shown in Fig. 4 [black squares in Fig. 11(a) for a 16-mm-long cell and black triangles in Fig. 11(b) for a 25-mm-long capillary tube].

In accordance with Fig. 10, the simulation results presented in Fig. 11 exhibit a maximum of the SXRL signal that is shifted to lower pressures when the target length is increased. The experimental results shown in Fig. 4 for the capillary tube exhibit the same behavior when the tube length is increased from 16 mm to 25 mm. One main difference between the gas cell and the capillary tube is the presence, in the case of the capillary, of a narrow peak close to 10 mbar observed both in the experiment and in the simulation at 25 and 30 mm target lengths, whereas at 16 mm, this peak is not apparent. This is the demonstration of the expected result that the influence of guiding is important mainly when the target length is large.

For the 8-mm and 16-mm gas cells, the simulation curves have a width at half maximum of about 20 mbar, in good agreement with experiment. However, the maximum reached by the simulation curves increases with the target length, whereas the experimental maximum at 16 mm is smaller than the value, reported in Fig. 5, obtained at 8 mm and 25 mbar. At high pressure, the absorption, not included in the simulation, can significantly reduce the output signal for the longest targets. However, the difference between experiment and simulation results at low pressure can only be explained by an overestimation of the theoretical gain at low pressure. One possible explanation is that at low pressure, Doppler broadening can begin to play a non-negligible role.

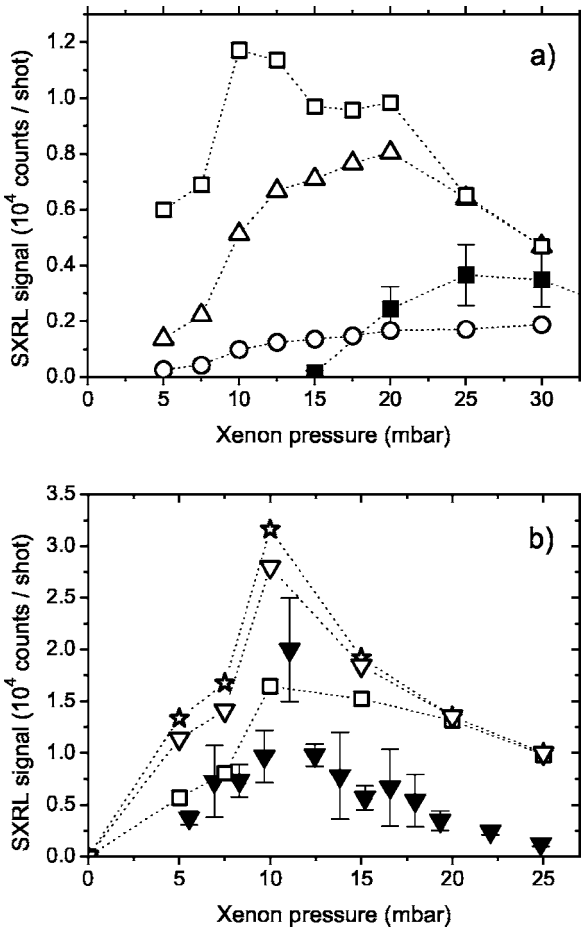

FIG. 11. Simulation results for the variation with pressure of the SXRL energy for (a) gas cells of length 4 mm (open circles), 8 mm (open triangles), and 16 mm (open squares) and (b) capillary tubes of lengths 16 mm (open squares), 25 mm (open triangles), and 30 mm (stars); experimental results (a) for a 16-mm-long cell (black squares) and (b) for a 25-mm-long capillary tube (black triangles).

V. CONCLUSIONS

We have presented experimental and simulation results for a laser source emitting at 41.8 nm and created by optical-field ionization of xenon gas inside a cell and a capillary tube. Target lengths large enough to measure the signature of reabsorption have been investigated, and the maximum length of amplifying medium achievable in the experimental conditions has been determined. In gas cells, without guiding, the maximum of the SXRL energy has been achieved at a pressure of 25 mbar and for a length of the amplifying plasma of 6–8 mm. It has been observed that the increase of the plasma length, obtained while reducing gas pressure, cannot compensate the fact that the local gain has its optimal value at 20–25 mbar. This optimal value for the pressure appears to be a robust value, reported in several previous publications [2,8,14], with different experimental conditions, and seems to be of general validity for xenon gas.

In the case of the capillary tube, the situation is quite different. The guiding of the ir beam allows one to reach much longer plasmas, increasing the length of the amplifying

medium at the optimal pressure by a factor of 4–5 and the SXRL energy emitted in the forward direction by nearly the same amount. A strong correlation between the efficiency of the guided ir transmission and the emitted SXRL energy has been found. The strong decrease of the guided ir transmission at high pressure induces a shift, compared to the cell case, of the optimum pressure to lower values, a narrow peak around 10 mbar having been identified. The strong influence of the guiding indicates that some enhancement in the SXRL energy is still possible by improving the guiding efficiency at higher pressure—for example, by using different material for the capillary walls.

A numerical code COFIXE, in which the local plasma properties are parametrized in terms of the maximum value of the ir intensity, has been elaborated. It has allowed us to calculate the SXRL amplification and transport over long distances in a reasonable computer time and to perform a direct quantitative comparison with experimental results. An excellent agreement has been obtained between experiment and theory for several features such as the divergence of the beam, the correlation between guided ir beam transmission and SXRL energy, and also the enhancement factor induced by guiding. On a quantitative level, on most of the observed quantities, the difference between theory and experiment is within a factor of 2, which seems extremely satisfactory taking into account the approximations used in the model.

ACKNOWLEDGMENTS

The authors acknowledge invaluable technical assistance from the laser support staff at Laboratoire d'Optique Appliquée, ENSTA. T.M. was supported by the European Commission under Contract No. HPMF-CT-2002-01554.

[1] B. Lemoff, G. Y. Yin, C. L. Gordon III, C. P. J. Barty, and S. E. Harris, Phys. Rev. Lett. **74**, 1574 (1995).
[2] S. Sebban, R. Haroutunian, Ph. Balcou, G. Grillon, A. Rousse, S. Kazamias, T. Marin, J. P. Rousseau, L. Notebaert, M. Pittman, J. P. Chambaret, A. Antonetti, D. Hulin, D. Ros, A. Klisnick, A. Carillon, P. Jaeglé, G. Jamelot, and J. F. Wyart, Phys. Rev. Lett. **86**, 3004 (2001).
[3] S. Sebban, T. Mocek, D. Ros, L. Upcraft, Ph. Balcou, R. Haroutunian, G. Grillon, B. Rus, A. Klisnick, A. Carillon, G. Jamelot, C. Valentin, A. Rousse, J. P. Rousseau, L. Notebaert, M. Pittman, and D. Hulin, Phys. Rev. Lett. **89**, 253901 (2002).
[4] D. J. Spence, A. Butler, and S. M. Hooker, J. Opt. Soc. Am. B **20**, 138 (2003).
[5] F. Dorchies, J. R. Marquès, B. Cros, G. Matthieussent, C. Courtois, T. Vélikoroussov, P. Audebert, J. P. Geindre, S. Rebibo, G. Hamoniaux, and F. Amiranoff, Phys. Rev. Lett. **82**, 4655 (1999).
[6] A. Butler, A. J. Gonsalves, C. M. McKenna, D. J. Spence, S. M. Hooker, S. Sebban, T. Mocek, I. Bettaibi, and B. Cros, Phys. Rev. Lett. **91**, 205001 (2003).
[7] A. Butler, A. J. Gonsalves, C. M. McKenna, D. J. Spence, S. M. Hooker, S. Sebban, T. Mocek, I. Bettaibi, and B. Cros, Phys. Rev. A **70**, 023821 (2004).
[8] T. Mocek, C. M. McKenna, B. Cros, S. Sebban, D. J. Spence, G. Maynard, I. Bettaibi, V. Vorontsov, A. J. Gonsavles, and S. M. Hooker, Phys. Rev. A **71**, 013804 (2005).
[9] *Laser Speckle and Related Phenomena*, Vol. 9 of *Topics in Applied Physics*, edited by J. C. Dainty (Springer-Verlag, Berlin, 1984).
[10] A. Klisnick *et al.*, J. Quant. Spectrosc. Radiat. Transf. **99**, 370 (2006).
[11] N. A. Andreev, B. Cros, L. M. Gorbunov, G. Matthieussent, P. Mora, and R. R. Ramazashvili, Phys. Plasmas **9**, 3999 (2002).
[12] M. V. Ammonosov, N. B. Delone, and V. P. Krainov, Sov. Phys. JETP **64**, 1191 (1986).
[13] G. J. Pert, J. Phys. B **32**, 27 (1999).
[14] T. Mocek *et al.*, Phys. Rev. Lett. **95**, 173902 (2005).
[15] G. J. Pert, J. Phys. B **29**, 619 (1990).
[16] G. J. Pert, J. Phys. B **34**, 881 (2001).
[17] W. Eissner *et al.*, Comput. Phys. Commun. **8**, 270 (1974).
[18] W. Eissner, Comput. Phys. Commun. **114**, 295 (1998).
[19] F. Strati and G. J. Tallents, Phys. Rev. A **64**, 013807 (2001).
[20] G. J. Pert, J. Opt. Soc. Am. B **11**, 1425 (1994).
[21] F. Lambert, G. Maynard, and J. Clerouin (private communication).
[22] Ph. Zeitoun *et al.*, Nature (London) **431**, 426 (2004).
[23] Center for X-Ray Optics, Berkeley Laboratory (http://www-cxro.lbl. gov/).